ELSEVIER

Biophysical Chemistry 72 (1998) 87–100

Biophysical Chemistry

Spark-to-wave transition: saltatory transmission of calcium waves in cardiac myocytes

Joel Keizer[a,*], Gregory D. Smith[b]

[a]*Institute of Theoretical Dynamics and Section on Neurobiology, Physiology and Behavior, University of California, Davis, CA 95616, USA*
[b]*Mathematical Research Branch, National Institute of Diabetes and Digestive and Kidney Diseases, National Institutes of Health, Bethesda, MD 20814, USA*

Revision received 5 January 1998; accepted 13 February 1998

Abstract

Using a modular approach, in which kinetic models of various mechanisms of calcium handling in cells are fine-tuned to in vivo and in vitro measurements before combining them into whole-cell models, three distinct modes of transmission of calcium waves in mature and immature frog eggs have been defined. Two modes of transmission are found in immature eggs, where the inositol 1,4,5-trisphosphate receptor (IP_3R) controls release of calcium from the endoplasmic reticulum (ER). The first mode corresponds to an excitable physiological state of the cytoplasm and results in solitary waves that can appear as circular or spiral waves in two dimensions with the wave speed proportional to the square root of the diffusion constant of calcium. A second mode occurs when the state of the cytoplasm is oscillatory and because of the small size of the buffered diffusion constant for calcium, the wave speed can appear to be weakly dependent on diffusion. In the mature frog egg, where the sperm-induced Ca^{2+} fertilization wave is a propagating front, the cytoplasm appears to be bistable and in this mode the wave speed is also proportional to the square root of the diffusion constant. Here we investigate a fourth mode of propagation for cardiac myocytes, in which calcium release from the sarcoplasmic reticulum (SR) is dominated by clusters of ryanodine receptors spaced at regular intervals. In myocytes a stochastically excitable myoplasm leads to the spontaneous production of calcium 'sparks' that under certain conditions can merge into saltatory waves with a speed proportional to the diffusion constant.

Keywords: Calcium oscillations; Diffusion; Calcium sparks; Kinetic model

1. Introduction

Calcium ions (Ca^{2+}) are an important second messenger in living cells [1]. The physiological role of Ca^{2+} signals is quite diverse, ranging from triggering hormonal release to the activation of egg cells by fertilization [2].

The Ca^{2+} signal is complex and adapted to the specialized needs of particular cell types. Indeed, the message carried by the cytosolic calcium concentration, $[Ca_i^{2+}]$, is often found to be transduced periodically – analogous to AC signals carried by electrical circuits. Since cells have a spatial extent and because

* Corresponding author. Tel.: +1 530 7520938; fax: +1 530 7527297; e-mail: jekeizer@ucdavis.edu

0301-4622/98/$19.00
PII S0301-4622(98)00125-2

Ca^{2+} can diffuse in both internal stores and in the cytosol, Ca^{2+} signals can also propagate as Ca^{2+} waves [4]. Ca^{2+} waves were first observed in the medaka eggs [3] and subsequently have been observed in a variety of cells types [5].

Intracellular Ca^{2+} waves have been characterized best in the immature *Xenopus laevis* oocyte [6] and in mature eggs from a variety of species [7,8]. Extensive theoretical work has been carried out in an effort to understand the basic biophysical mechanisms underlying these waves [9–15], which are primarily due to Ca^{2+} release from internal stores. This work has focused on continuum reaction diffusion equations with underlying mechanisms that are deterministic and has uncovered three distinct modes of transmission of Ca^{2+} waves: (1) solitary and spiral waves that occur when the physiological state of the cytoplasm is excitable [10,14]; (2) repetitive wave trains and spiral waves that occur when the cytoplasm is oscillatory [13–15] and (3) traveling fronts (sometimes called 'tides') that occur when the cytoplasm is bistable [16,17]. The first two of these mechanisms have been proposed to be responsible for Ca^{2+} waves observed in the immature *Xenopus laevis* oocyte, while the third mechanism seems to describe the fertilization Ca^{2+} wave in the mature *Xenopus* egg.

The continuum description of Ca^{2+} waves is appropriate when Ca^{2+} release sites are distributed with a continuous density on a distance scale that is small compared with the distance scale of observation. These conditions appear to hold for most observations of waves in both immature and mature *Xenopus* eggs. This is despite the fact that the waves are composed of elementary, stochastic release events called Ca^{2+} 'puffs' [18] that can be seen at low levels of inositol-1,4,5-trisphosphate (IP_3), the second messenger that potentiates Ca^{2+} release from the IP_3 receptor (IP_3R) Ca^{2+} channel in the endoplasmic reticulum (ER).

Recent calculations suggest that the discrete nature of puffs may play a role in the transition between abortive and propagating waves in these cells [19].

The situation is more complicated in cardiac myocytes, in which release occurs via ryanodine receptor Ca^{2+} channels (RyR) located in a regular array of release sites in the sarcoplasmic reticulum (SR) [20,21]. Under normal physiological conditions, the release of Ca^{2+} from these sites is a localized event referred to as a Ca^{2+} 'spark' since they show up as bright spots in confocal images of fluorescent indicators [22].

The mode of transmission of Ca^{2+} waves in cardiac myocytes appears to differ in two important ways from the three modes described above for *Xenopus laevis* oocytes. First, the regular structure of release sites produces a spatio-temporal correlation among release events due to that fact that Ca^{2+} release at one site can be triggered via Ca^{2+}-induced Ca^{2+} release (CICR) from Ca^{2+} released at a neighboring site. Second, the stochastic nature of the release site kinetics appears to play a significant role in initiation and propagation of the waves. Here we develop a kinetic model of a RyR release site in cardiac myocytes and use it to explore the properties of Ca^{2+} waves mediated by a regular array of stochastic release sites. Our simulations reveal a new mode of propagation with a wave speed that is proportional to the Ca^{2+} diffusion constant, rather than its square root, as is found for reaction-diffusion waves in an excitable or bistable cytoplasm. The regular separation of release sites leads to a saltatory movement of the wave front that is slower than the analogous continuum reaction diffusion wave.

2. Review of continuous, deterministic Ca^{2+} waves

The continuous, deterministic description of Ca^{2+} waves uses reaction diffusion equations containing terms for Ca^{2+} diffusion and continuously distributed kinetic terms to account for calcium-handling mechanisms within the cytoplasm. Writing the rates of Ca^{2+} uptake and release from internal stores as J_{up} and J_{rel}, respectively, and neglecting influx of Ca^{2+} from the external medium, the balance equations for Ca^{2+} can be written

$$\partial c/\partial t = D\nabla^2 c + J_{rel} - J_{up} \tag{1}$$

$$\partial c_s/\partial t = D_s\nabla^2 c_s - (J_{rel} - J_{up})/\alpha \tag{2}$$

where $c = [Ca_i^{2+}]$, c_s is the concentration of Ca^{2+} in the internal store (ER or SR), and the factor α takes into account differences in size and buffering of the cytoplasm and the store [30]. The diffusion constants include buffering, as well, and so are *effective* diffusion constants [30].

The nature of the uptake and release terms depends on the types of mechanism being considered. Although this is not necessary [17,23–25], in almost all previous work the release and uptake mechanisms are taken to be uniformly distributed throughout space. Moreover, kinetic mechanisms are assumed to be deterministic so that Eq. (1) and Eq. (2) are partial differential equations of the usual sort.

The dynamics of the underlying release and uptake mechanisms play a large role in determining whether or not Eq. (1) and Eq. (2) support Ca^{2+} waves and their mode of transmission. Fig. 1 illustrates three distinct physiological states of the cytoplasm that have been proposed to underlie Ca^{2+} waves in *Xenopus laevis* oocytes: excitable, oscillatory and bistable. In these cells, Ca^{2+} release occurs from the ER via the IP_3R and uptake into the ER occurs through sarcoendoplasmic reticulum calcium (SERCA) 2b Ca^{2+} ATPase pumps. The three physiological states of the cytoplasm correspond to three different modes of transmission of Ca^{2+} waves.

All three physiological states can be derived from a simplified two-variable version of the De Young–Keizer model [26,27], as described in the legend to Fig. 1. The three panels show the nullclines for those equations, i.e. the curves on which the time derivative of each variable vanishes. The intersection of these curves, shown by the filled square, gives the steady-state solutions of these equations. The rich dynamical behavior exhibited by this model is due to the N-shape of the Ca^{2+} nullcline [28], which is reminiscent of that for the well-characterized FitzHugh–Nagumo model [29]. Fig. 1A shows an excitable physiological state, which is typified by the fact that an initial deviation from the stable steady state that exceeds a threshold value, gives rise to a large amplitude increase in $[Ca_i^{2+}]$ before it returns to its steady-state value. This is shown by the superimposed heavy line, which is a representative trajectory in the phase space. Fig. 1B shows an oscillatory physiological state, in which the intersection of the nullclines occurs at the inner branch of the N-shaped nullcline. This is a stable limit-cycle type oscillation that circles around the unstable steady state in the direction shown by the arrow. Finally, Fig. 1C illustrates the nullclines for a bistable system. There the nullclines intersect three times, producing two stable steady states.

The dynamical behaviors shown in Fig. 1 lead to

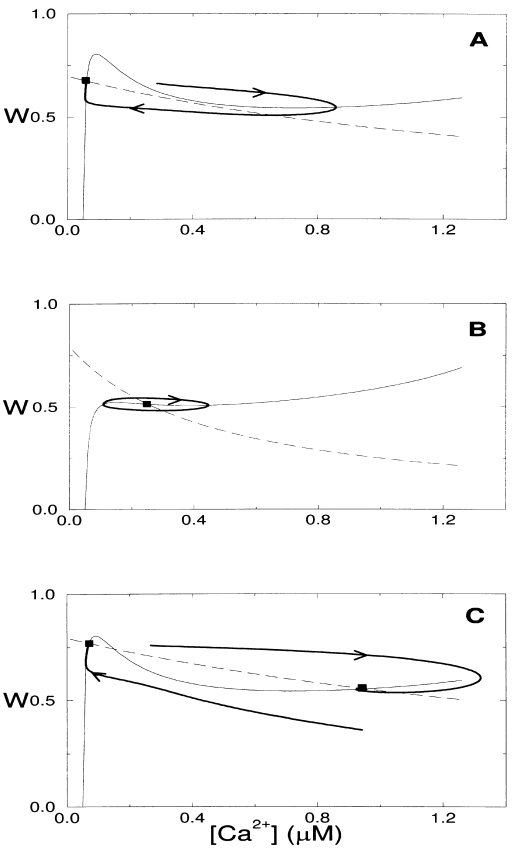

Fig. 1. Nullclines for simplified IP_3-based Ca^{2+} dynamics underlying three modes of Ca^{2+} waves. The equations for the two-variable model ($c = [Ca_i^{2+}]$ and w, the fraction of IP_3R not inactivated) are given below. The Ca^{2+}-nullcline is the full line, the dashed line is the w-nullcline, and the heavy full line is a representative trajectory. Steady states are indicated by the filled squares. (1A) Nullclines for excitable dynamics (parameters given below), which produces a solitary traveling or spiral wave in the presence of Ca^{2+} diffusion. The single steady state is stable. (1B) Nullclines for oscillatory dynamics (same parameters as below, except $[IP_3] = 0.5\ \mu M$; $d_2 = 1.05\ \mu M$, $d_5 = 0.082\ \mu M$, $[Ca_t^{2+}] = 2.0\ \mu M$, and $v_2 = 0.11/s$), which give rise to repetitive wave trains or spiral waves. The steady state is unstable. (1C) Nullclines for bistable conditions (same parameters as below, except $[IP_3] = 0.5\ \mu M$), which gives rise to a traveling wave front. Two of these steady states are stable. The ordinary differential equations for c and w are: $dw/dt = (w^{\infty}(c) - w)/\tau(c)$ and $dc/dt = (c_1\ (v_2 + v_1(wc/(c + d_5))^3)(c_s(c) - c) - v_3c^2/(k_3^2 + c^2))$ with $w^{\infty}(c) = (d_2I/(I + d_3))/(c + (d_2(I + d_1)/(I + d_3)))$, $\tau(c) = (1/(c + (d_2(I + d_1)/(I + d_3))))(1/a < _2)$, and $c_s(c) = ([Ca_t^{2+}] - c)/c_1$. Parameter values are $I = 0.5\ \mu M$, $a_2 = 0.2/\mu M/s$, $c_1 = 0.18$, $c_0 = 2.5\ \mu M$, $d_1 = 0.13\ \mu M$, $d_2 = 5\ \mu M$, $d_3 = 0.94\ \mu M$, $d_5 = 0.2\ \mu M$, $v_1 = 6/s$, $v_2 = 0.075/s$, $v_3 = 0.9/\mu M/s$, $k_3 = 0.1\ \mu M$. A detailed explanation of the model and parameters can be found elsewhere [26,27].

three different types of Ca^{2+} waves. The excitable state can give rise to a Ca^{2+} wave that propagates from an initial local increase in Ca_i^{2+} above the threshold value [10,14]. In one spatial dimension this gives rise to a solitary plane wave with a wave speed proportional to $\sqrt{D}$, whereas in two dimensions it yields a circular wave. Inhomogeneous initial conditions can lead to spiral waves analogous to those seen in the Belousov–Zhabotinsky reaction [29]. The oscillatory state in Fig. 1B gives rise to wave trains, which in two dimensions are expanding target patterns, and to spiral waves as well [14]. These waves are somewhat more complicated, however, because of the effective value of the diffusion constant of calcium is quite small due to the presence of Ca^{2+} buffers in the cytosol [13,14]. This produces a potential role for the diffusion of IP_3, which can set the phase of the oscillations at any point in space. Since Ca^{2+} diffusion is slow, under certain conditions the speed of the waves can be largely independent of *D*. However, asymptotically in time the speed of these waves can increase linearly in time in proportion to *D*. It has recently been shown that this can be explained using Burgers' equation [15].

Finally, the bistable state illustrated in Fig. 1C provides an example of the classical traveling wave front in the generalized bistable model [29]. As with the excitable case, the wave speed is proportional to $\sqrt{D}$. It has been proposed that the Ca^{2+} fertilization wave in *Xenopus* eggs is caused by this sort of mechanism [17].

3. Stochastic model of Ca^{2+} sparks

Our stochastic model of Ca^{2+} sparks is based on the phenomenon of adaptation exhibited by isolated RyRs in phospholipid bilayers [31]. We have previously used a four-state model of the RyR to quantitatively reproduce the rapid activation and slow adaptation of the channel observed in those experiments [32]. To achieve agreement with experiments both in bilayers and cardiac myocytes in vitro (see below), we explore here an extension of our earlier model that includes six states, and adjust its properties so that it mimics both the in vitro measurements of isolated channels and the in vivo measurements of Ca^{2+} sparks.

A diagram of the states and kinetic steps in the model is given in Fig. 2. The states O_1 and O_2 are open states, whereas C_0–C_3 are closed, and the forward direction of all of six kinetic steps (labeled A–F) are dependent on Ca^{2+}. Step B, however, is dependent on domain Ca^{2+}, which represents the localized Ca^{2+} concentration, $[Ca_d^{2+}]$, that accumulates within a few microseconds at the mouth of open Ca^{2+} channels [34,35]. In the in vitro measurements with Cs^+ as the charge carrier $[Ca_d^{2+}] = [Ca_i^{2+}]$, whereas in vivo $[Ca_d^{2+}] >> [Ca_i^{2+}]$. In the absence of explicit experimental information, we take $[Ca_d^{2+}] = 10\ \mu M$. This value gives spark maxima that are within a factor of two of what is estimated experimentally [21] and a unitary current for the open state that is in agreement with experiment (2 pA).[1] The rate constants used in our calculations are listed in Table 1.

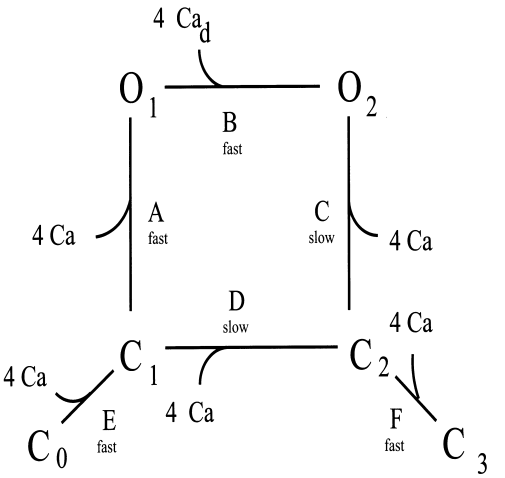

Fig. 2. State diagram of the model stochastic RyR-based Ca^{2+} release site. Note the domain Ca^{2+}-mediated transition from state O_1 to O_2 (process B). $[Ca_d^{2+}]$ takes the value of 10 μM when Ca^{2+} is the current carrier and is otherwise equal to the bulk Ca^{2+} concentration. The structure and rate constants of this model were chosen to reproduce (1) the peak (P_o^{peak}) and plateau (P_o^{plat}) open probability measure with Cs^+ as the charge carrier [31] (see Fig. 3) and (2) the open and closed dwell times of an isolated RyR measured in vitro ($\tau_o < 1$ ms) and in vivo (τ~15 ms). See Table 2.

A judicious selection of parameters was made so that the model release site satisfies two types of experimental constraint. First, with Cs^+ as the current carrier, the model is constrained to fit the kinetic experiments on adaptation. In particular, the peak

[1] It is of course possible to increase the value of c_s simply by decreasing the value of ν_1^* (see Table 3 and Eq. (5)).

Table 1

Parameters for model release site

Parameter	Value	Unit
k_a^+	5×10^5	$\mu M^{-4}/s$
k_a^-	9600	/s
k_b^+	5×10^4	$\mu M^{-4}/s$
k_b^-	1.3×10^4	/s
k_c^+	3.333	$\mu M^{-4}/s$
k_c^-	66.67	/s
k_d^+	5000	$\mu M^{-4}/s$
k_d^-	1.235	/s
k_e^+	5×10^4	$\mu M^{-4}/s$
k_e^-	2.5×10^5	/s
k_f^+	5×10^4	$\mu M^{-4}/s$
k_f^-	3×10^6	/s

open probability (rise time on a millisecond time scale) and subsequent relaxation to a plateau value (second time scale) are shown as a function of $[Ca_i^{2+}]$ in Fig. 3A. The agreement of both curves with experiment is comparable with that for our previous four-state model [32]. Second, with the elevated value of $[Ca_d^{2+}]$, corresponding to the in vivo measurements of Ca^{2+} sparks, the model was constrained to mimic experimental estimates of the open, closed and refractory times of a release site [21,22]. The calculated dwell times for basal levels of Ca^{2+} are shown in Table 2. The open and refractory times are in general agreement with experiment. Fig. 3B shows the predicted alteration in the peak and plateau open fractions when Ca^{2+} is the charge carrier. This generalizes our previous four-state model, which cannot predict both the experiments on bilayers (with Cs^+ as the charge carrier) and those on sparks (with Ca^{2+} as the charge carrier).

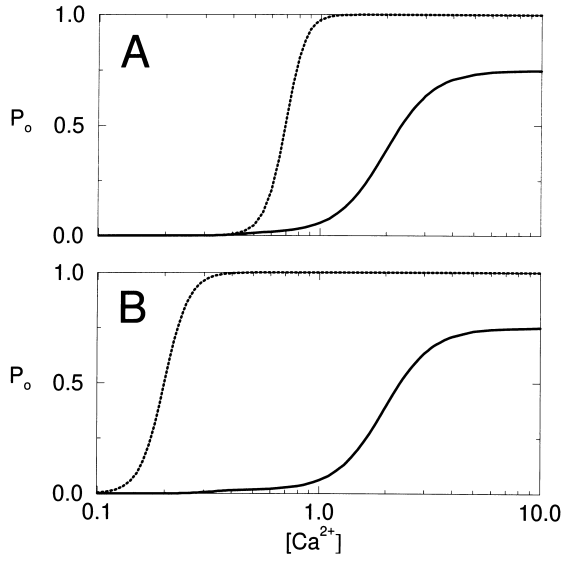

Fig. 3. Peak (P_o^{peak}) and plateau (P_o^{plat}) open probability of the stochastic RyR-based Ca^{2+} release site in the absence (A) and presence (B) of domain Ca^{2+}, calculated using the parameters in Table 1. In the presence of domain Ca^{2+}, the steady-state open probability (P_o^{plat}, *solid line*) of the model RyR increases slightly in the range of 0.2–0.4 μM bulk Ca^{2+}. The leftward shift in the transient open probability (P_o^{peak}, *dotted line*) in B indicates that a step increase in bulk Ca^{2+} activates the model release site more strongly in the presence (B) of domain Ca^{2+} than in its absence (A).

The six-state model in Fig. 2 can be greatly simplified since four of the steps are relatively fast. Using the assumption of rapid equilibration of these steps [32], we have reduced the model to the three- and two-variable models illustrated in Fig. 4. In the three-variable model the open state (O) is $O_1 + O_2$, the closed state (C) is $C_0 + C_1$ and the refractory state (R) is $C_2 + C_3$. In the two-state model the non-refractory state, N, is given by C + O in the three-state model. We find that the kinetic behavior on the time scale of sparks is similar for all three models.

An illustration of the stochastic behavior of the reduced three-variable model is given in Fig. 5. Using the reduced transition rates for this model, which inherit an explicit dependence on both $[Ca_i^{2+}]$ and $[Ca_d^{2+}]$ from the parent six-state model (cf. Ref. [31]), we have simulated transitions among the three states using standard methods for a Markov process [33]. At basal values of $[Ca_i^{2+}]$, the closed state, *C*, dominates, with only an occasional brief opening (cf. Table 2). When $[Ca_i^{2+}]$ is raised to 0.5 μm, the refrac-

Table 2

Dwell times of stochastic model release site

Symbol	$[Ca_d^{2+}] = [Ca_i^{2+}]$/ $[Ca_d^{2+}] = 10\ \mu M$	Description
τ_o	0.1 ms/15 ms	Open
τ_c	1.0×10^4 s/1.0×10^4 s	Closed
τ_n	1.0×10^5 s/9.1×10^3s	Non-refractory
τ_r	810 ms/810 ms	Refractory

Dwell times for the stochastic RyR-based Ca^{2+} release site under resting conditions ($[Ca_d^{2+}]$ 0.1 μM) both in vitro ($[Ca_d^{2+}] = [Ca_i^{2+}]$ to simulate Cs^+ as the current carrier [31]) and in vivo ($[Ca_d^{2+}]$ set to 10 μM to simulate Ca^{2+} as the current carrier).

Table 3

Parameters for model myocyte

Parameter	Value	Unit
v_{pump}	10.0	μM/s
k_{pump}	0.184	μM/s
v_1	10.0	μM/s
v_1^*	200	μM/s
v_{leak}	0.01	μM/s
$[Ca_d^{2+}]$	1.2	μM
α	0.1	–
$D = D_s$	60	$\mu m^2/s$

tory state, R, which is punctuated by brief openings, now dominates.

4. Deterministic simulations

To help to differentiate the implications for wave propagation of the stochasticity of release sites from their regular arrangement in space, we first carried out deterministic simulations. In these simulations the release sites were separated on a linear array by a fixed distance, $d = 2.0$ μm, to represent their association with the t-tubule structures of myocytes. We have used the two-state reduction of our stochastic model and the release and uptake rates have the following forms:

$$J_{rel} = (v_1 f_O + v_{leak})(c_s - c) \quad (3)$$

$$J_{up} = v_{pump} c^4 / (k_{pump}^4 + c^4) \quad (4)$$

where f_O is the instantaneous fraction of the maximal release rate for the site and v_{leak} is the leak rate constant. The uptake rate has the form measured for Ca^{2+} pumps into the SR of myocytes [36]. The functional form of f_O comes from the reduction of the six-state model and is given in Appendix A. In these simulations both the uptake rate, J_{up}, and the leak rate, were distributed uniformly in space.

The spatial structure of the model is illustrated in Fig. 6, along with spatial profiles of both $[Ca_i^{2+}]$ and $[Ca_s^{2+}]$ over the 200 μm domain used in the calculations. The simulations were carried out using the partial differential equations, Eqs. (1) and (2), and the expressions for the release and uptake rates given above and in Appendix A. The equations were integrated using a Crank–Nicolson algorithm for diffusion and Euler's method for the spatially local terms ($\Delta t = 0.001$ ms, $\Delta x = 0.1$ μm) with periodic boundary conditions. Since an individual release site (length = $\Delta x = 0.1$ μm) takes the place of the release capacity of a 2.0-μm segment in the continuous model, the release rate of a site is rescaled by a factor of 20 to $v_1^* = 200$ μM/s. Although it is not necessary, in the calculations presented here we have assumed further that the diffusion constant of Ca^{2+} in the SR is the same as that in the cytoplasm ($D = D_s$) and that initially the quantity $\alpha c_s + c = [Ca_t^{2+}]$, which is a measure of the total concentration of Ca^{2+}, is independent of position. This is equivalent to solving only Eq. (1) and calculating the store content from the relationship $c_s = ([Ca_t^{2+}] - c)/\alpha$.

The top panel of Fig. 6 shows a snapshot ($t = 0.2$ s) of the highly structured profile of $[Ca_i^{2+}]$ in the wave. The release sites, indicated by the tick marks on the space axis, are in the non-refractory (but closed) state in front of the wave, in the non-refractory (but mostly open) state at the peak of the wave, with the refractory state building up in the tail. The wave of Ca^{2+} in the cytosol is accompanied by a depletion wave in the SR (bottom panel). When observed over time, the wave front progresses in a saltatory fashion, with rapid release occurring at individual sites via CICR. This

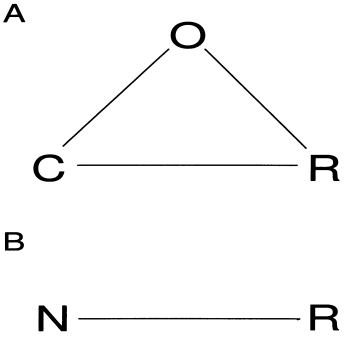

Fig. 4. Two simplifications of the full model of the RyR-based Ca^{2+} release site obtained by 'reducing' the complete model in Fig. 1 using the fact that certain transitions are fast. The three-state reduction (*A*) combines states C_0 and C_1 into a single closed state, C; the two open states, O_1 and O_2 into a single open state, O; and C_2 and C_3 into a refractory state, R. The two-state reduction (*B*) further combines C and O into a single non-refractory state, N. The dynamic behavior of all three models is similar.

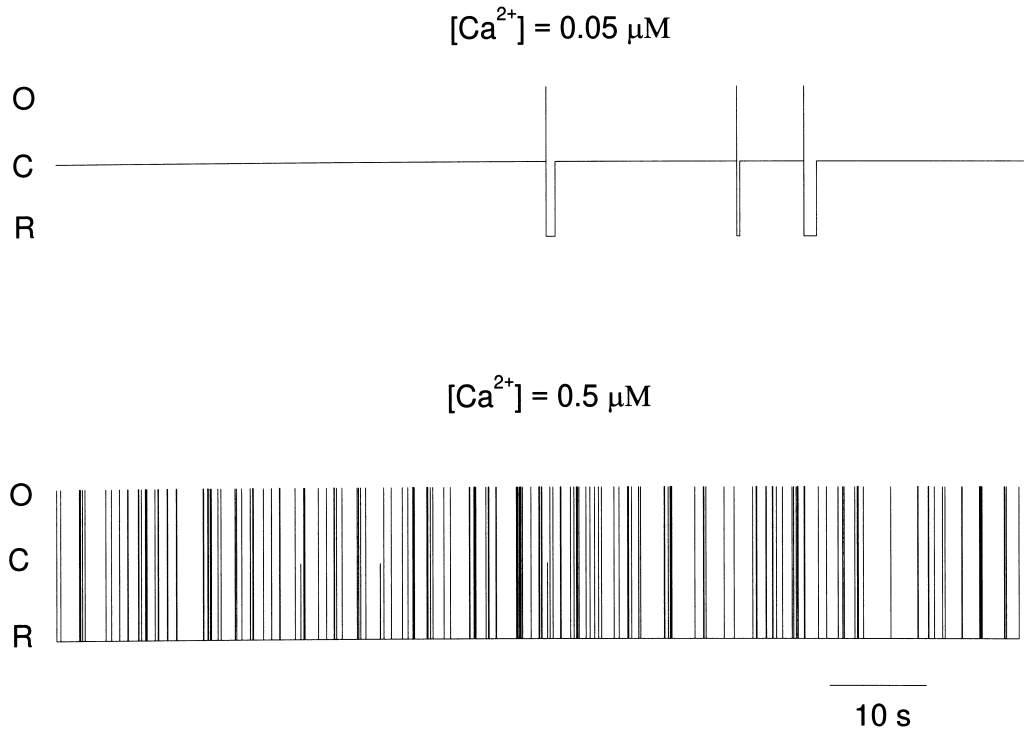

Fig. 5. Stochastic transitions calculated using three-state reduction (see Fig. 4) of the model RyR-based release site and its dependence on bulk Ca^{2+} concentration.

is followed by diffusion of Ca^{2+} to neighboring sites where CICR triggers further release.

A space-time plot (sometimes called a 'waterfall plot') of the same wave is given in Fig. 7. Time increases in the downward vertical direction and space is indicated horizontally. The wave was initiated by opening three sites around $x = 0$, which raises $[Ca_i^{2+}]$ locally to about the basal level (0.06 μM). The speed of the wave, v, is given by the magnitude of the slope of the wave front, which in this simulation is $v = 120$ μm/s. The punctate nature of the release sites is apparent in the fine structure of the image, in which color indicates the value of $[Ca_i^{2+}]$. The dimension (approximately 2 μm) and duration (approximately 100 ms) of the sparks are similar to those seen in cardiac myocytes [22]. The amplitude, which is about 0.6 μM, is about a factor of two higher than that estimated from the non-ratio imaging dyes that are required to visualize sparks.

In contrast to the modes of Ca^{2+} wave transmission considered in Section 2, the speed of the spark-mediated wave, v, depends linearly on the diffusion constant of Ca^{2+}, D. This is shown in Fig. 8, where the wave speeds for simulations like that in Fig. 7, but with D varied, are plotted. The slight curvature in this plot is due to the approach to the continuum limit for large values of D/d and propagation failure when $D/d \approx 8$ μm/s. Since the parameters of this model would lead to an excitable myoplasm like that in Fig. 1A if the release sites were spread with a continuous spatial density, one might have expected v to be proportional to $\sqrt{D}$. Simulations of this sort, which mimic the continuum limit, are given in Fig. 9. They verify the expected proportionality of v to $\sqrt{D}$, showing that it is the discrete nature of the release sites that is responsible for this novel dependence of the wave speed on the diffusion constant.

5. Stochastic simulations

We have combined stochastic simulations of Ca^{2+} release sites, like that in Fig. 5, with the Ca^{2+} balance equations, Eqs. (1) and (2), to obtain a spatio-temporal

representation of the spark-to-wave transition. In these simulations the release rate from an individual site is a stochastic variable given by:

$$\tilde{J}_{\text{site}} = \tilde{v}_1^*(c_s - c) \tag{5}$$

where $\tilde{v}_1^*$ is a random variable that takes the values 0 or v_1^* depending on whether the site is open or closed (see Fig. 2). The leak and uptake rates are calculated deterministically in these calculations, as is the diffusion of Ca^{2+}.

Deterministic calculations with the three-variable model (not shown) similar to those in the previous section, demonstrate that two conditions are necessary for saltatory Ca^{2+} wave propagation: (1) a single site must be able to release a sufficient amount of Ca^{2+} so that diffusion can spread the release to neighboring sites and (2) CICR must be fast enough that the site can release the necessary amount of Ca^{2+} before it becomes refractory. Both of these conditions also are necessary for stochastic wave propagation, but both are dependent on the stochastic behavior of the release site.

In order to obtain simulations that propagate Ca^{2+} waves and support isolated Ca^{2+} sparks, we have

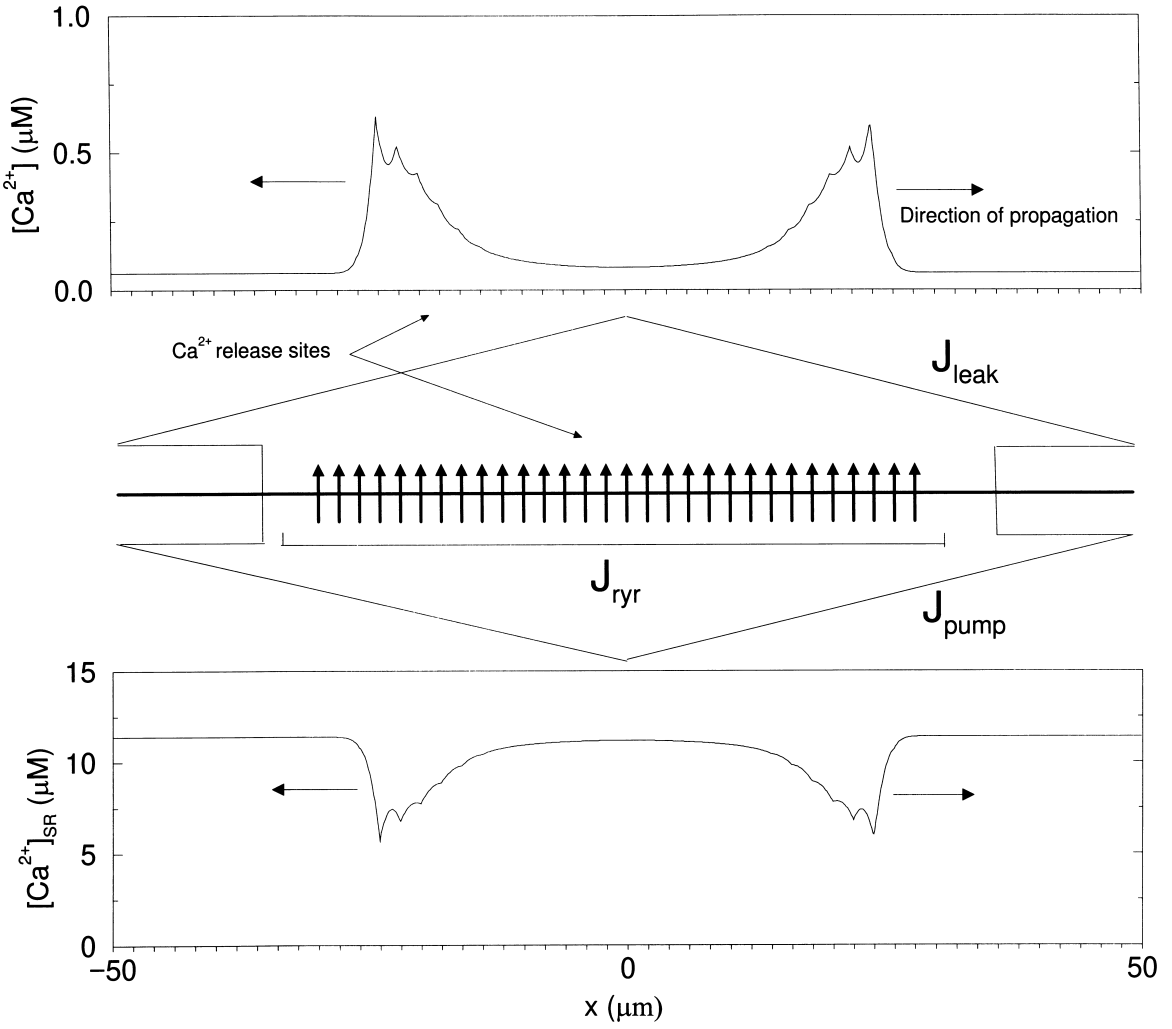

Fig. 6. Diagram of model components and fluxes, with the central panel a blow-up of a release-site showing localized release of Ca^{2+} from the SR into the myoplasm. The model represents a longitudinal cross section of a cardiac myocyte and includes (1) Ca^{2+} diffusion, (2) regularly-spaced Ca^{2+} release sites and (3) either deterministic (as here) or stochastic behavior of the release sites. Parameters are as in Tables 1 and 3.

found that it suffices for the underlying equations to exhibit a stochastic analogue of excitability. This is illustrated in Fig. 10, where the time records of the states of a release site are shown for three fixed values of $[Ca_i^{2+}]$. Near basal concentrations of Ca^{2+} ($[Ca_i^{2+}] = 0.07\ \mu M$), the site is almost always closed

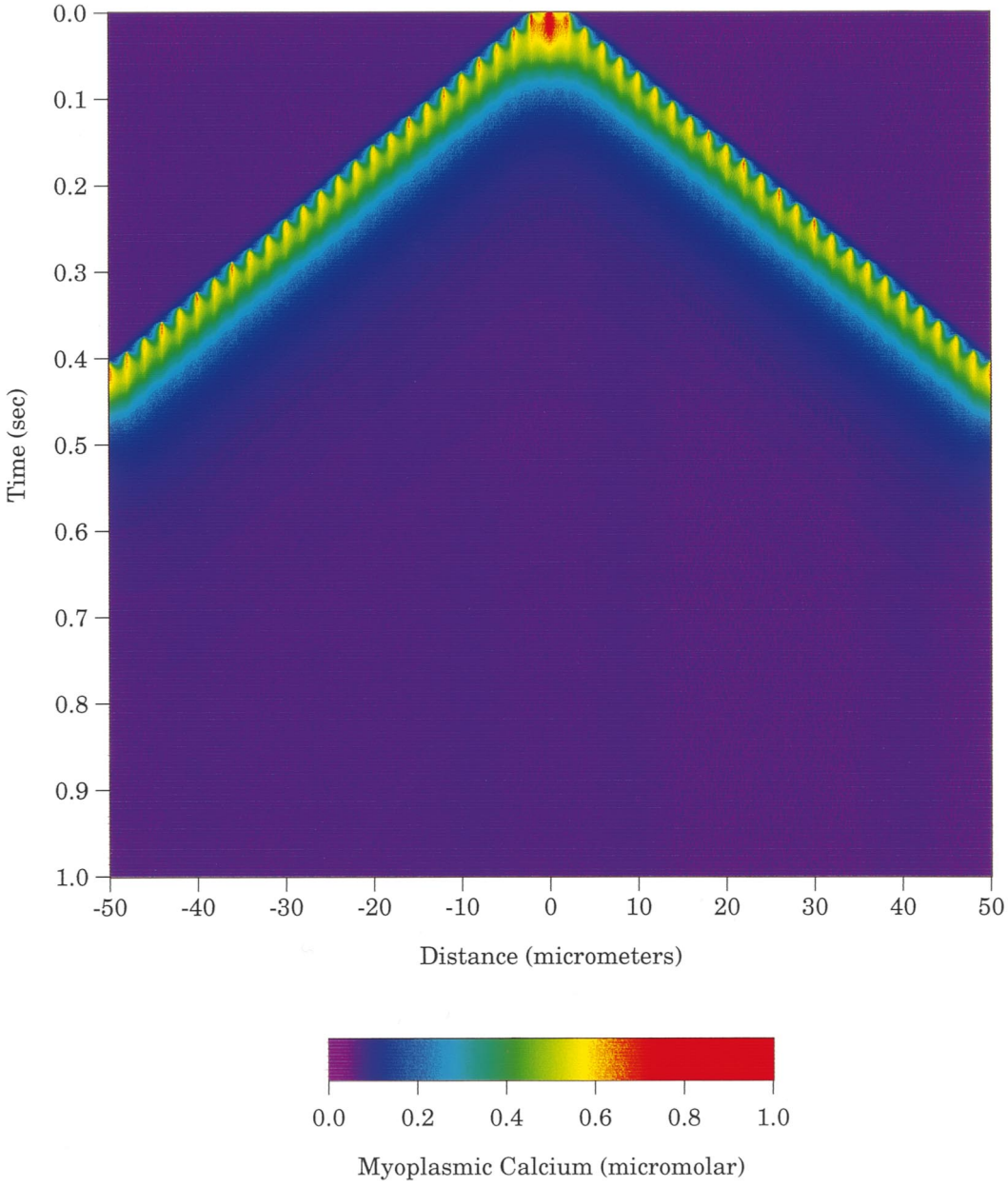

Fig. 7. Simulated line-scan image of $[Ca_d^{2+}]$ in the myoplasm of a cardiac myocyte with color bar representing Ca^{2+} concentration; space is represented on the horizontal axis and time on the vertical. The parameters are as in Tables 1 and 3. Slope of the wave front gives the wave speed, $v = 120\ \mu m/s$. Simulations employ the two-state release site model ($N \leftrightarrow R$) along with a Ca^{2+} leak, SERCA pumps, and Ca^{2+} diffusion, as described in the text.

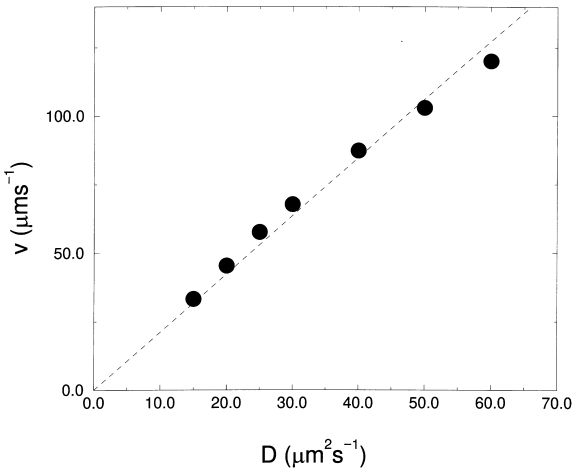

Fig. 8. Wave speed, v, versus the diffusion coefficient of Ca^{2+}, D, for release sites separated by 2.0 μm, as shown in Fig. 7. The wave speed is a linear function of D; slope of dashed line is 2.12/μm.

and, thus, this concentration is below the threshold for producing a spark. Raising $[Ca_i^{2+}]$ slightly to 0.10 μm, however, makes an enormous difference in the stochastic behavior, allowing brief openings (approx. 10–20 ms duration) that are comparable with the open time of sparks. Thus when $[Ca_i^{2+}]$ reaches this value the site is 'primed,' greatly increasing the probability that a spark will be produced at the site. The

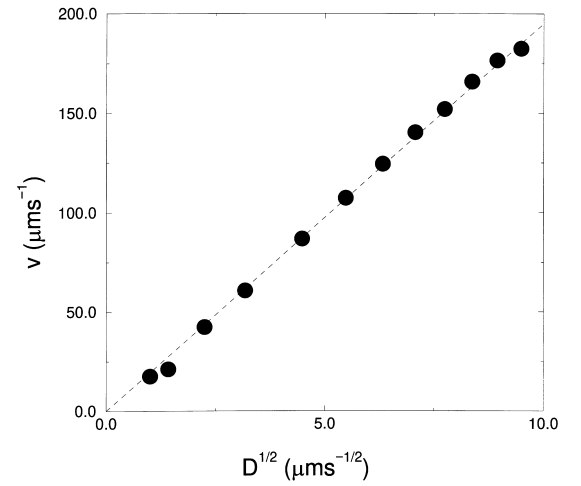

Fig. 9. Wave speed, v, versus square root of the diffusion coefficient of Ca^{2+}, D, for the continuum limit version of the simulation in Figs. 7 and 8. In these simulations $d = 0.1$ μm with the same release and re-uptake rates per unit length as in Figs. 7 and 8. The wave speed is a linear function of $D^{1/2}$; slope of dashed line is 19.5s$^{-1/2}$.

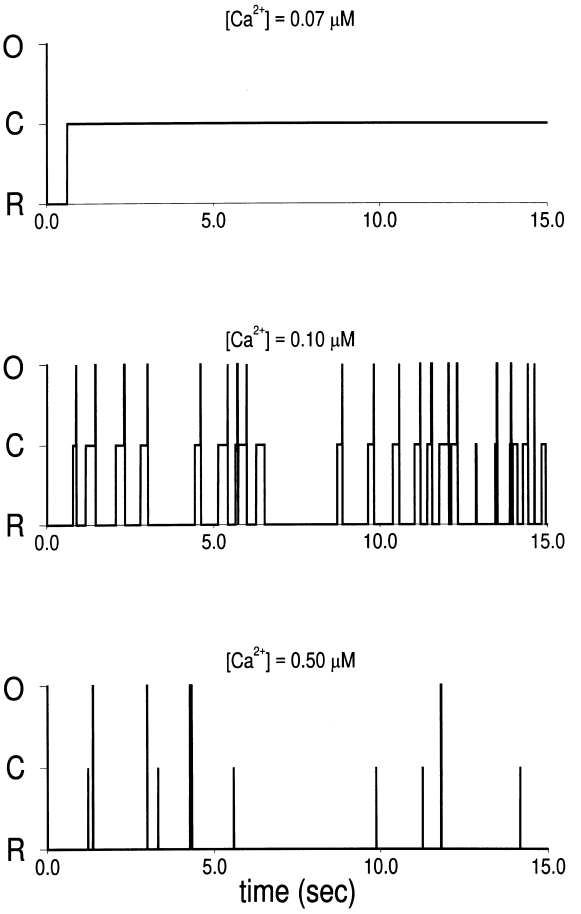

Fig. 10. Stochastic realizations of the three-state reduction of the Ca^{2+} release site (see Fig. 4) for the indicated values of $[Ca_i^{2+}]$. Parameter values are as in Table 1, except $K_e = k_e^- / k_e^+ = 0.001$ μM^4; simulations initiated with the site open. Transitions between the closed and open state in the central panel represent a site that is 'primed' for spark production.

value of $[Ca_i^{2+}]$, however, rises rapidly after an opening to a peak concentration of the order of $[Ca_i^{2+}] = 0.50$ μM. The bottom panel of Fig. 10 shows that at this value of $[Ca_i^{2+}]$, refractory periods of 2–5 s occur, which inhibits the site from producing additional release events until $[Ca_i^{2+}]$ again falls closer to basal levels. It is this sequence of activities for a release site, i.e. a small increase in $[Ca_i^{2+}]$ above a threshold, causing a large release of $[Ca_i^{2+}]$ followed by a refractory period, that we refer to as *stochastic excitability*, since it is analogous to the deterministic excitability illustrated in Fig. 1A.

To achieve stochastic excitability in the model, it

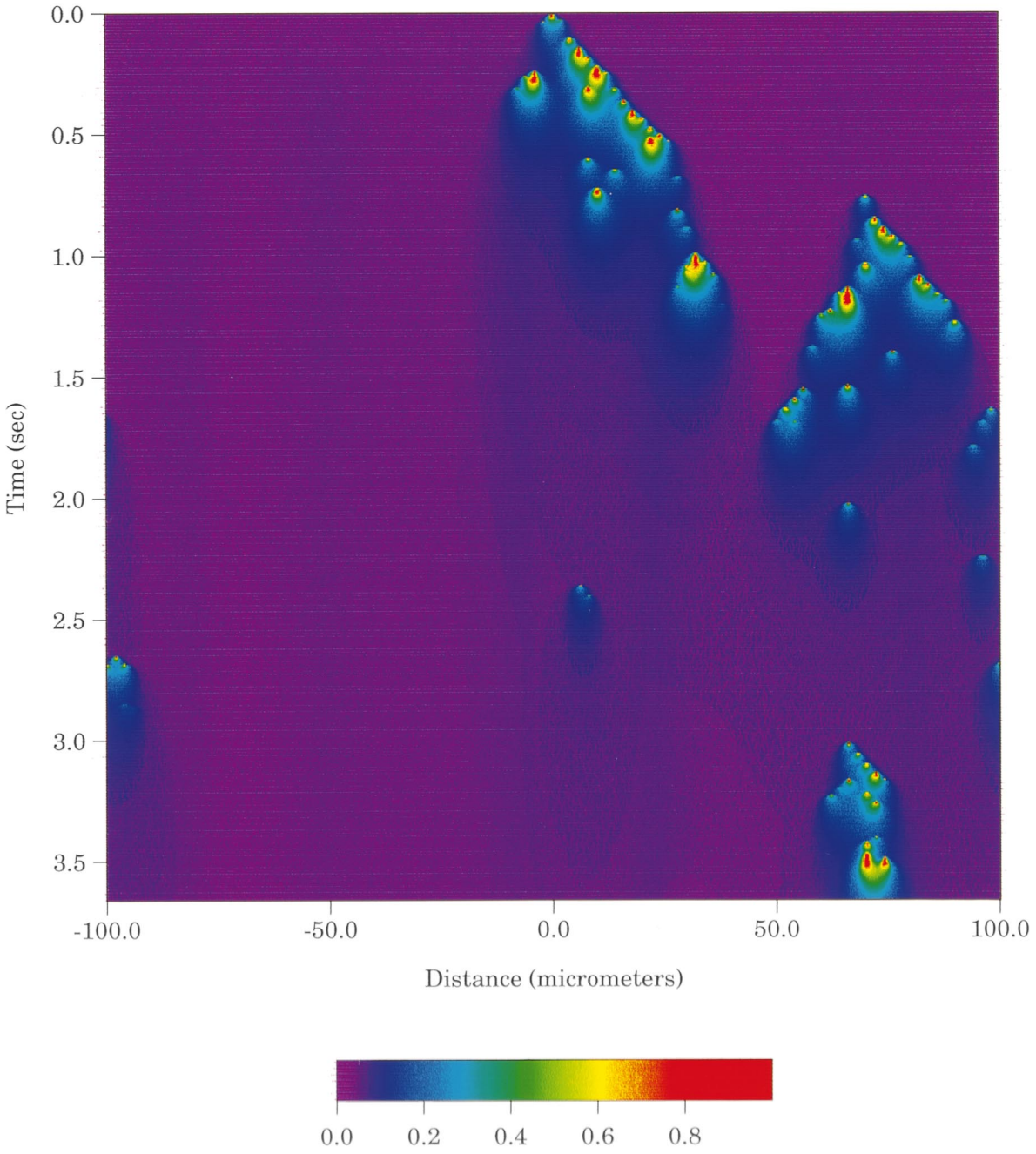

Fig. 11. Simulation of Ca^{2+} sparks and propagating waves of SR Ca^{2+} release in a Ca^{2+}-overloaded cardiac myocyte. Ca^{2+} is plotted as a function of both space (horizontal axis: 200 μm in length) and time (vertical axis: total of 3.5 s in length). The simulation begins with $[Ca_i^{2+}] = 0.04$ μm and all Ca^{2+} release sites closed (C), except for one release site (center) that is open (O). SR Ca^{2+} release from this site leads to a local Ca^{2+} elevation, which initiates a propagating Ca^{2+} wave via activation of neighboring release sites (uppermost inverted V; a velocity of 45 μM/s is given by slope). This Ca^{2+} wave eventually terminates ($t = 0.7$ s), but later ($t = 0.8$ s) a spontaneous Ca^{2+} release event initiates a pair of waves propagating in opposite directions. Note the presence of Ca^{2+} sparks of various amplitudes that do not lead to propagating Ca^{2+} waves. Parameters are as in Tables 1 and 3, except $K_e = k_e^-/k_e^+ = 0.001$ μM^4, $D = 30$ $\mu m^2/s$, $v_{pump} = 2$ μM/s, $v_{leak} = 4 \times 10^{-4}$ μM/s and $\Delta t = 1 \times 10^{-4}$ ms.

has been necessary to lower the value of the equilibrium constant $K_e = k_e^- / k_e^+$ from 5 to 0.001 μM^4. This has the effect of increasing the probability of a site being in state C_1 at low values of $[Ca_i^{2+}]$, which increases the rate of transition between the closed and open states (see Fig. 2), as is evident in the central panel of Fig. 10. It is crucial that the release site just in front of the wave have a high probability of making an open transition before the Ca^{2+} released by the site at the front is either taken up into the SR or diminishes via diffusion. This does not occur when K_e = 5 μM^4. Not only is a site open too often at $[Ca_i^{2+}]$ = 0.50 μM (see Fig. 5), but time records that are comparable with the middle (threshold) panel in Fig. 10 are not observed until $[Ca_i^{2+}] \approx 0.30$ μM. This threshold is simply too high for a spark-type release event to trigger release from its neighbors.

A full stochastic simulation with the same array of release sites used for the deterministic calculations is shown in Fig. 11. The simulation was initiated by setting the state of the release site at the origin to open while the remaining sites were all closed, in line with the dwell times in Table 2. The stochastic nature of the release events is evident in the figure. Whereas the initial event succeeds in evoking a spark similar to that seen in the deterministic calculation in Fig. 7, it does not induce both neighboring sites to fire, and the site to the right fires only after a delay. The right-moving branch of the wave is composed of an irregular array of spark events with a front that is, nonetheless, rather well-defined until the wave terminates after about 0.65 s. The succeeding small elevation of $[Ca_i^{2+}]$ above basal in this spatial region (blue portion of the color bar), however, primes some of these sites for subsequent spark production. At about the same time, a spontaneous spark occurs near $x = 70$ μm, which leads to a rather ragged wave that propagates in both directions. Later, a wave is initiated by another spark and aborts in the same region of space. Sparks of a variety of sizes, depending on the length of the open time of their release site, are seen to occur without initiating a wave.

6. Discussion

Our simulations suggest that Ca^{2+} spark-mediated waves in cardiac myocytes are distinctly different from Ca^{2+} waves in *Xenopus laevis*. First, the movement of the wave is saltatory, reminiscent of the propagation of action potentials down myelinated nerve fibers [37]. This feature is in good agreement with the punctate nature of the wave front that is revealed via fluorescence imaging [21]. A more detailed analysis of saltatory wave propagation [25] reveals that saltatory propagation occurs only when the ratio of the mean open time of a release site (τ) is small compared with the mean time for diffusion between sites (d^2/D). Continuous waves, on the other hand, are observed when $D\tau/d^2 >> 1$. That analysis shows further that the value of the dimensionless parameter, c^*d/σ, where σ is the amount of free Ca^{2+} that appears in the cytoplasm when a site is open and c^* is the threshold for CICR, dictates whether or not waves can propagate.

Second, our deterministic simulations suggest that the wave speed is proportional to the diffusion constant of Ca^{2+}, D, rather than $\sqrt{D}$, as expected from a continuous, uniform density of release sites. In fact, it is not difficult to show that the wave speed for a saltatory wave should be proportional to D/d [25]. This makes precise earlier observations that increasing the distance between localized areas of Ca^{2+} release and increasing the diffusion constant have a similar effect on Ca^{2+} waves [12]. Finally, our stochastic simulations suggest that in order to propagate waves of the sort observed experimentally in myocytes, the underlying physiological state of the cytoplasm must be excitable in the stochastic sense described in the previous section. These waves are not classical reaction-diffusion type waves and have properties that merit further theoretical investigation.

The main features of our simulations are quite similar to what is observed in cardiac myocytes under conditions of Ca^{2+} overload, i.e. pre-exposure of the cells to high external Ca^{2+} concentrations. Under these conditions, Cheng and colleagues [21] report the coexistence of isolated Ca^{2+} sparks and waves. Moreover, the wave front sometimes exhibits a ragged appearance, and weak right or left moving waves have been reported. Waves with relatively ragged tails and relatively sharp fronts appear to be the rule, as also seen in the simulation in Fig. 11. Collisions of Ca^{2+} waves in myocytes initiated by electrical stimulation have shown that the cytoplasm immediately behind a wave is refractory with a recovery time

of about 0.45 s. This is comparable with the refractory time in our model and is of the order of the delay in the reappearance of sparks at given sites in Fig. 11.

The experimental parameter in our simulations that controls the spark-to-wave transition is the total free cell calcium concentration, $[Ca_t^{2+}]$. In fact, $[Ca_t^{2+}]$ acts as a bifurcation parameter that determines if Ca^{2+} sparks can reinforce each other and propagate as waves. When $[Ca_t^{2+}]$ is low, i.e. when the SR store is not overloaded, only isolated, spontaneous sparks are observed in the simulations. For higher values of $[Ca_t^{2+}]$, corresponding experimentally to Ca^{2+} overload, both Ca^{2+} sparks and Ca^{2+} waves are observed, as shown in Fig. 11. This aspect of the model is in qualitative agreement with experiment [21].

Our simulations lend support to the suggestion [21] that sparks are an important event underlying Ca^{2+} waves in cardiac myocytes. However, more work will be necessary in order to relate quantitatively the stochastic features of the present model to experiment. In particular, additional simulations need to be performed to help understand the transition between the physiological state of the myoplasm, in which only isolated sparks are seen, and the Ca^{2+} overload state, in which sparks and waves coexist in the same cell. Calculations with a simplified caricature of the model presented here, which we have dubbed the 'fire-diffuse-fire' model, suggest that the threshold for wave propagation is governed by a single, dimensionless parameter [25]. Furthermore, this model leads to propagation failure via a series of period-doubling bifurcations (in the time interval between firing of successive sparks at the wave front) that ultimately terminate in a chaotic state. A stochastic version of the fire-diffuse-fire model, in which the state of a release site varies between refractory and non-refractory, would undoubtedly have very different properties, but might provide a simpler understanding of the nature of this threshold in the myocyte.

Acknowledgements

This work was supported by NSF grant BIR 9214381 and NIH grant R01 RR10081 to JK, the Agricultural Experiment Station at UC Davis, and an IRTA Fellowship to GS. We gratefully acknowledge numerous discussions with Dr. Heping Cheng and Dr. John Pearson, which have helped guide our work on Ca^{2+} sparks.

Appendix A. Rate of release from a site

The explicit form for the rate of release from a site depends on the fraction of the maximal release rate, f_O. Using algebra like that in [32], we find that:

$$f_O = \frac{Nc^8}{K_e K_a}\left(1+\frac{c_d^4}{K_b}\right)\Big/B \tag{6}$$

with

$$B = 1+\frac{c^4}{K_e}\left(1+\frac{c^4}{K_a}\left(1+\frac{c_d^4}{K_b}\right)\right) \tag{7}$$

In Eq. (6) N represents the fraction of the release site in the non-refractory state, N, which satisfies the kinetic equation:

$$dN/dt = -\rho_0 N + \rho_1(1-N) \tag{8}$$

where

$$\rho_0 = \left(\frac{k_c^- c^8 c_d^4}{K_e K_a K_b}+\frac{k_d^+ c^8}{K_e}\right)\Big/B \tag{9}$$

$$\rho_1 = (k_c^+ c^4 + k_d^-)\frac{K_f}{K_f + c^4} \tag{10}$$

The equilibrium constants are defined by $K_i = k_i^-/k_i^+$ with i = a,b,c,e,f.

References

[1] M.J. Berridge, Nature 361 (1993) 315.
[2] J. Keizer, Y.-X. Li, J. Rinzel, S. Stojilkovic, Mol. Biol. Cell 6 (1995) 945.
[3] E.B. Ridgeway, J.C. Gilkey, L.F. Jaffe, Proc. Natl. Acad. Sci. USA 74 (1977) 623.
[4] L.F. Jaffe, Proc. Natl. Acad. Sci. USA 88 (1991) 9883.
[5] L.F. Jaffe, Cell Calcium 14 (1993) 736.
[6] J. Lechleiter, D. Clapham, Cell 69 (1992) 283.
[7] R. Nuccitelli, D.L. Yim, T. Smart, Dev. Biol. 158 (1993) 200.
[8] S.A. Stricker, V.E. Centoze, R.F. Melendez, Dev. Biol. 166 (1994) 34.
[9] G. Dupont, A. Goldbeter, BioEssays 14 (1992) 485.

[10] A. Atri, J. Admunson, D. Clapham, J. Sneyd, Biophys. J. 65 (1993) 1727.
[11] J. Sneyd, S. Girard, D. Clapham, Bull. Math. Biol. 55 (1993) 315.
[12] G. Dupont, A. Goldbeter, Biophys. J. 67 (1994) 2191.
[13] M.S. Jafri, J. Keizer, Proc. Natl. Acad. Sci. USA 91 (1994) 9485.
[14] M.S. Jafri, J. Keizer, Biophys. J. 69 (1995) 2139.
[15] M.S. Jafri, J. Keizer, Bull. Math. Biol. 59 (1997) 1125.
[16] J. Sneyd, J. Keizer, M.J. Sanderson, FASEB J. 9 (1995) 1463.
[17] J. Wagner, Y.-X. Li, J.E. Pearson, J. Keizer, Biophys. J., submitted.
[18] I. Parker, Y. Yao, Proc. R. Soc. Lond. B 246 (1991) 269.
[19] A.E. Bugrim, A.M. Zhabotinsky, I.R. Epstein, Biophys. J. 73 (1997) 2897.
[20] P.S. Shacklock, W.G. Wier, C.W. Balke, J. Physiol. (London) 487 (1995) 601.
[21] H. Cheng, M.R. Lederer, W.J. Lederer, M.B. Cannell, Am. J. Physiol. (Cell Physiol. 39) 270 (1996) C148.
[22] H. Cheng, W.J. Lederer, M.B. Cannell, Science 262 (1993) 740.
[23] G. Dupont, J. Pontes, A. Goldbeter, Am. J. Physiol. (Cell Physiol. 40) 271 (1996) C1390.
[24] G.D. Smith, Thesis, University of California, Davis (1996).
[25] J. Keizer, G.D. Smith, S. Ponce-Dawson, J.E. Pearson, Biophys. J., in press.
[26] G. De Young, J. Keizer, Proc. Natl. Acad. Sci. USA 89 (1992) 9859.
[27] Y.-X. Li, J. Rinzel, J. Theor. Biol. 166 (1994) 461.
[28] Y.-X. Li, J. Keizer, S. Stojilkovic, J. Rinzel. Am. J. Physiol. (Cell Physiol. 38) 269 (1995) C1079.
[29] J.D. Murray, Mathematical Biology, Springer, Berlin, 1989, pp. 232, 277, 328.
[30] J. Wagner, J. Keizer, Biophys. J. 67 (1994) 447.
[31] S. Györke, M. Fill, Science 260 (1993) 807.
[32] J. Keizer, L. Levine, Biophys. J. 71 (1996) 3477.
[33] J. Keizer, Statistical Thermodynamics of Nonequilibrium Processes, Springer, NY, 1987, p. 228.
[34] G.D. Smith, J. Wagner, J. Keizer, Biophys. J. 70 (1996) 2527.
[35] A. Tripathy, G. Meissner, Biophys. J. 70 (1996) 2600.
[36] J.W.M. Bassani, R.A. Bassani, D.M. Bers, J. Physiol. (London) 476 (1994) 279.
[37] R. Fitzhugh, Biophys. J. 2 (1962) 11.